The effects of mistuning on Fan flutter

M. Vahdati
Imperial College London
Mechanical Engineering
Department
Exhibition Road, London SW7
2AZ, UK
m.vahdati@imperial.ac.uk

L. Salles
Imperial College London
Mechanical Engineering
Department
Exhibition Road, London SW7
2AZ, UK
l.salles@imperial.ac.uk

ABSTRACT

The aim of this paper is to study the effects of mistuning on fan flutter. The computations are based on a three-dimensional, whole assembly, time-accurate, viscous, finite-volume compressible flow solver. The unsteady flow cases are computed as Reynolds-averaged Navier–Stokes, with the basic assumption that the frequencies of interest are sufficiently far away from the frequencies of turbulent flow structures. The overall solution method is implicit, with second-order accuracy in space and time. A rig wide-chord fan blade, typical of modern civil designs, was used as the benchmark geometry for this study. There are 20 blades in the fan assembly. A random pattern frequency mistuning was used in most of analysis undertaken in this paper. The 1F mode shapes are the same for all mistuned blades. The objectives of this work are:

1. To check if the introduction of mistuning would bring the experimental and computed flutter boundaries closer
2. To explain how mistuning provide stability
3. Establish a relationship between mistuning and damping
4. Provide a data base which can be used in future for testing simple mistuning models

NOMENCLATURE

f	blade natural frequency, Hz
f_r	reduced frequency, fc/V
m	mass flow rate
m_{ref}	normalised corrected mass flow rate
p	static pressure
p_0	stagnation pressure
r	radius
r_t	rotor tip radius
V	velocity into rotor blades
Φ	inter-blade phase angle
θ	tangential coordinate
ω	rotor angular velocity
Ω	rotor non-dimensional angular velocity ($\omega 2\pi r_t/a_o$)

INTRODUCTION

It is well known that mistuning can have significant effect on fan flutter. The vast majority of turbomachinery blade mistuning studies have been conducted using only the effects of structural coupling. However, aerodynamic coupling between blades can have significant effects on the stability and blade forced response amplitudes. The significance of the aerodynamic coupling effects has been shown in recent literature. For example, Kielb et al. [1,2]and Miyakozawa[3] investigated the effects of aerodynamic coupling on both flutter and forced response using the single family of modes approach. The results suggested that the mistuning effects on flutter and forced response are dependent on the structural coupling levels. Campobasso et al. [4] conducted mathematical studies of flutter and forced response including the aerodynamic coupling effects assuming that the effect of the aerodynamic force is due to the blade motions of immediate neighbours. Sladojevic et al. [5] studied the correlation between the aerodynamic blade-to-blade coupling in mistuned bladed disk assemblies and the level of forced response. The analysis showed that the amplification factors were greatly increased due to aerodynamic coupling. He et al. [6] investigated the effects of aerodynamic coupling on both flutter and forced response problems using the tuned system modes to calculate the unsteady aerodynamic forces. For the case studied, aerodynamic coupling showed significant effects on the vibration amplitudes. All of these studies considered only blade frequency mistuning.

THE AERODYNAMIC COMPUTATION METHOD

The calculations in this paper were performed with the AU3D code written in Imperial College and developed over many years with support from Rolls-Royce [7]. The computations are performed using a three-dimensional, whole assembly, time-accurate, viscous approach. The unsteady flow cases are computed as Reynolds-averaged Navier–Stokes, with the basic assumption that the frequencies of interest are sufficiently far away from the frequencies of turbulent flow structures. The overall solution method is implicit, with second-order accuracy in

space and time. The current computations use the one-equation Spalart–Allmaras turbulence model [8]. The parameters in Spalart–Allmaras have been adjusted on previous fans to get good agreement near the stability limit; the parameters are held constant in all the present work. The resulting CFD code has been used over the past 20 years for flows at off design conditions with a good degree of success [9, 10, 11].

TEST CASE AND STEADY FLOW

A rig wide-chord fan blade, typical of modern civil designs, was used as the benchmark geometry for this study. The rig was used extensively to study flutter. There are 20 blades in the fan assembly. More details of test case can be found in [9]. **Fig. 1** compares the calculated and measured speed line for the fan used in this report for a tip Mach number close to sonic. For this speed the non-dimensional fan speed is Ω =0.89. The pressure ratio and mass flow are seen to be in adequate agreement.

The speedline is terminated to the left by the instability line and to the right is shown the normal working line. It should be noted from **Fig. 1** that the instability both measured and calculated can either be stall/surge or flutter, with flutter occurring over a narrow range of fan rotational speed, referred to as 'flutter bite'. The calculations, based on the known frequency and mode of vibration show instability due to flutter at somewhat higher mass flow rate than those measured. The higher computed mass flow for instability is attributed to the presence of some mechanical damping and mistuning in the real fan which is wholly omitted in the present calculations. The trend is well predicted, notably the flutter bite (i.e.,instability at increased throttle area) around the sonic speedline. One of the aims of this work is to see if the introduction of mistuning would bring the experimental and computed flutter boundaries closer and the level of mistuning required for this purpose.

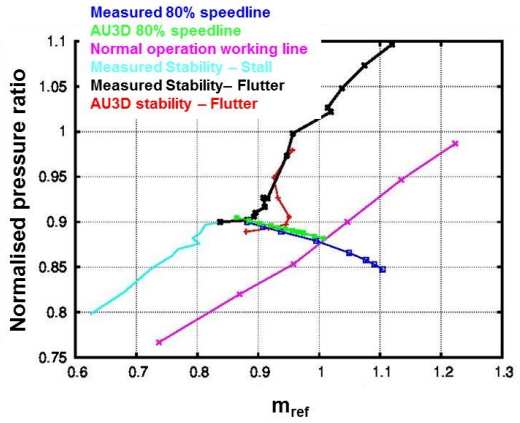

Fig 1. Performance plot for the model fan used in this investigation

It should be pointed out that the calculation in **Fig. 1** is for a complete fan, with outlet guide vanes and engine-section stators and that it includes an intake upstream of the fan. The intake was present for the measurements and the comparison must include the appropriate upstream boundary. The intake can decrease or increase stability, depending on the length, since the waves upstream of the rotor are reflected back from the intake plane and the phasing is critical [12]. Although the results in **Fig. 1** includes the intake to allow comparison with measurement, later calculations in this report assume no reflections, corresponding to infinitely long intake and exhaust ducts. The removal of reflection is achieved in the calculations by coarsening the computation mesh upstream and downstream of the rotor.

Fig. 2 shows the constant speed characteristic at Ω=0.89 for which flutter was observed during rig test.

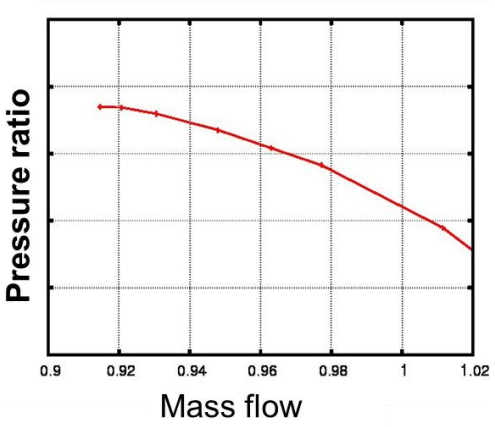

Fig 2: Constant speed characteristic at part speed

Fig 3a shows contours of isentropic Mach number in the blade-to-blade surface at 90% span for mass flow of m=0.93 when the relative velocity onto the rotor tip is close to sonic, Ω =0.89. There is a well-developed supersonic region downstream of the leading edge, terminated by a shock at about 20% chord. Fig. 3b shows the variation of static pressure along the blade at 90% height for different mass flows at Ω =0.89. It is seen from this plot that for all the operating points considered at this speed, the shock is expelled. However, the shock moves forward and becomes stronger as the mass flow decreases. Moreover, it can be seen from this plot that the pressure is nearly uniform along the pressure surface and nearly uniform downstream of the shock on the suction surface.

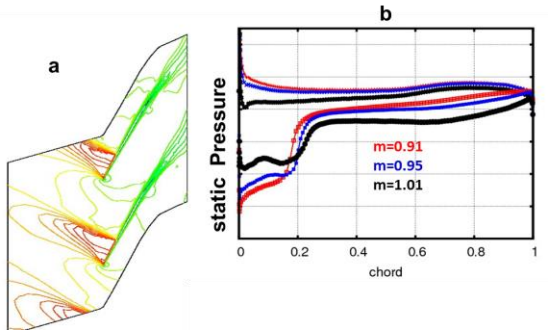

Fig 3: Typical view of steady flow at the speed. (a) Mach number contours at 90% height for m=0.93; (b) Static pressure variations along the blade at 90% height

MECHANICAL MODEL

The mode shape and frequency used here were obtained from an FE package and were interpolated onto the CFD grid. The mode shapes remain fixed during computation. It is an underlying assumption that the mechanical mode is unaffected by the aerodynamic forces. Only the 1st mode (1F), shown in **Fig. 4a**, is considered at this stage.

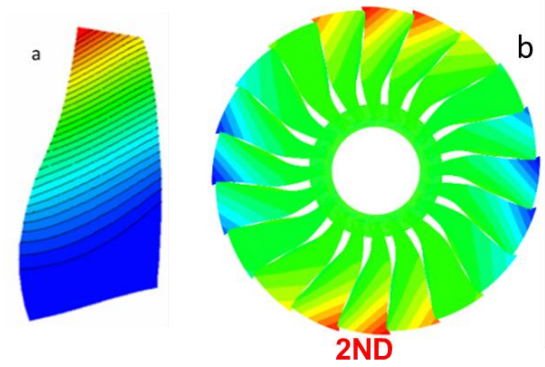

Fig. 4: (a) View of 1F mode shape for 1 blade, (b) Expaned 1F/2ND mode shape for whole assemblt

The usual approach in flutter computations is to expand the mode shape of **Fig. 4a** for all the blades and Nodal Diameters (ND) of interest. **Fig. 4b** shows the 1F/2ND expanded mode. This method of expansion will be referred to as ND expansion of mode shape in the rest of this paper. Unsteady flutter computations begin from a steady state solution by exciting all the nodal diameters of interest. The amplitude of motion is large enough to be well outside the noise range, but small enough for the unsteady flow to be represented as linear; the imposed tip displacements are typically of the order of 0.3% of blade chord at the tip. The time history of displacement of each ND is tracked to establish whether that ND is stable or unstable. The stability of each mode is determined from the time history of the modal displacement. **Fig. 5a** shows typical time history of displacement of a stable mode (black curve) and an unstable mode (red curve). Aerodynamic damping is evaluated by fitting a line to the modal displacement amplitudes. The slope of the line on a log scale yields the logarithmic decrement (logdec) with a positive value corresponding to positive aerodynamic damping and negative value corresponding to negative damping. **Fig. 5b** shows damping plotted against ND for mass flow of, m=09.3. It is seen from this plot that for this case 2ND mode is unstable.

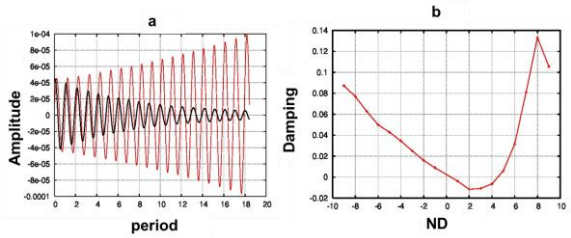

Fig 5: (a) Time history of displacement for a stable ND (black) and unstable ND (red); (b) Damping for m=0.93 as a function of ND

The approach shown above cannot be used for mistuned assemblies, as the expansion method used does not differentiate between blades (it can only distinguish between NDs), and hence one cannot assign different frequencies to blades. Therefore, in the absence of mode shapes for the whole assembly, a new approach for expansion of mode shapes is required. In the approach taken here, it is assumed that the fan assembly displacement is made of 20 different 1F modes, for which mode N corresponds to blade N having displacement while the displacement for all the other blades being zero. Modes 1, 5 and 13 are shown in **Fig. 6**. Therefore, with this approach, it is assumed that there is no structural coupling between blades and coupling is only through air. At time T=0.0, only blade 1 is excited and the time history of all the blades are tracked. This method of mode shape expansion will be referred to as blade expansion in the rest of the paper.

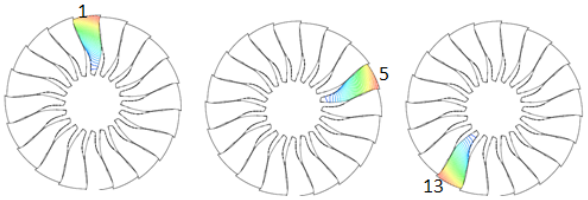

Fig 6: Alternative form of mode shape expnsion; blades with no contours have zero displacement in the mode

Before proceeding to mistuned computations, the blade expansion of the mode shape was checked. **Fig. 7** shows the time history of displacement of displacement for 4 blades around the assembly for a stable point (m=0.98) and an unstable point (m=0.93). It should be noted that at T=0.0 only blade 1 is excited.

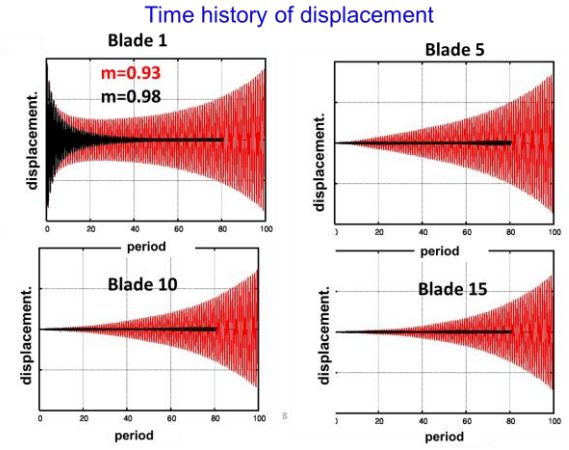

Fig 7: Time history of displacement for 4 blades around the annulus, m=0.93 unstable; m=0.98 stable

It can be seen from **Fig. 7** that initially (up to 10 periods of vibration) the time history of displacement for both mass flows is similar. However, for m=0.93 the initial disturbance of blade 1 is able to travel around the annulus and excite other blades and cause flutter, whereas for m=0.98 the initial excitation is unable to cause vibration on other blades. This can be clearly seen from **Fig. 8** which shows displacement plotted as a function of blade number for 5 instants of time during the motion.

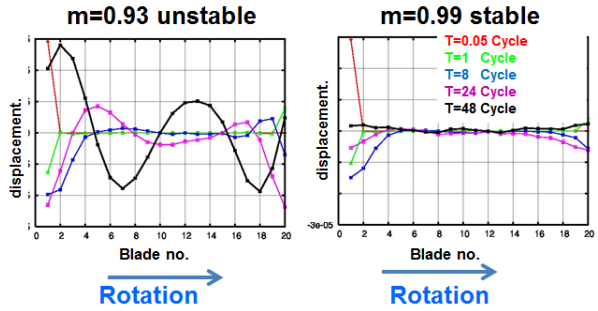

Fig 8: Time history of displacement as a function of blade number

It is seen from this plot that at T=0.05 cycle (red curve) and T=1 cycle (green curve) the displacement is much localised (around blade 1) and does not differ between the two mass flows. At T=8 cycles (blue curve) it is still hard to distinguish between the two mass flows cases, although for m=0.93more blades (19, 18 and 17) show vibration. At T=24 cycle (pink curve), the characteristic of vibration is totally different between the two mass flow cases and all the blades for m=0.93 show response. At T=48 cycles (black curve), a clear 2ND pattern is developed for m=0.93, whereas for m=0.98 all the vibration has died out. This can be clearly seen from **Fig. 9** which shows the time history of displacement after 90 cycles.. It can also be seen from this plot that, for m=0.93, the travelling wave moves by two blades in the direction of rotation in ¼ of cycle, which is consistent with a 2ND travelling wave pattern.

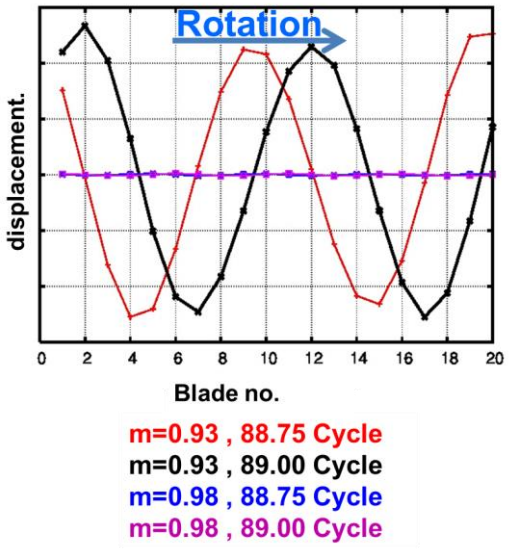

Fig 9: Time history of displacement as a function of blade number

Snapshots of unsteady pressure on the suction surface and the casing at two instants of time are shown in **Fig. 10**. It is seen from these plots that initially (T=0.05 Cycle), the disturbance is confined around blade 1 (Top dead centre) but after 80 cycles a clear 2ND pattern has developed. This clearly shows that aero coupling is sufficient to determine the least stable ND.

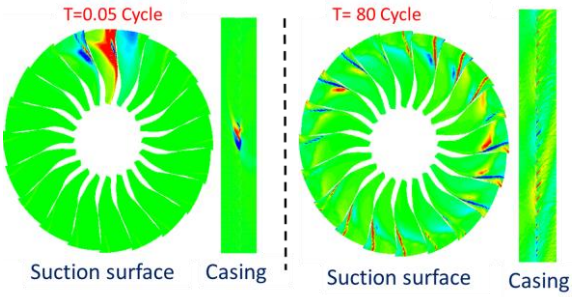

Fig 10: Instantaneous variations of unsteady pressure on the suction surface and the casing for m=0.93

Fig. 11 shows the comparison of damping between the ND and blade expanded mode shapes. For the ND expanded mode shapes, the damping curve is for a 2ND pattern. For the blade expanded mode shape computations, the unstable points at m=0.93 and m=0.91 converge to a 2ND pattern. As can be seen from time history plots of **Fig. 7**, obtaining damping from the time histories is not straight forward. In the strategy used in this work, for the stable points damping has been obtained from time history of blade 1 between 60-80 cycles, and for the unstable points damping has been obtained from time history of displacement over the last part of (80+ cycle) motion. For the unstable points, as the number of cycles increases the damping of all the blades

converge to the same value. It is seen from this plot that, as expected, the two approaches give similar values for damping. The blade expanded mode shape strategy needs around 100 cycle of vibration for accurate computations of damping, whereas ND expanded mode shape strategy require around 10 cycle of vibrations. Therefore, blade expanded mode shape strategy is not advisable for tuned computations. Also shown in **Fig. 7**, is the overall damping of the blade 1 which can be interpreted as the sum of damping for all NDs.

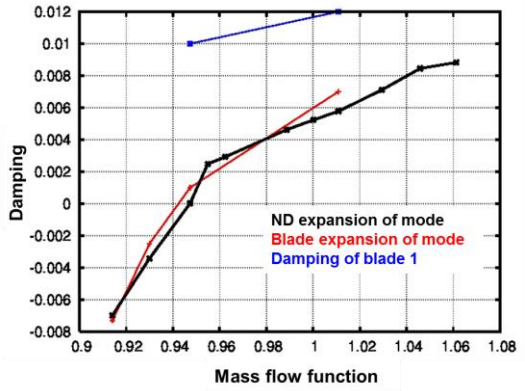

Fig 11: Comparison of damping between ND and blade expend mode shape.

MISTUNED COMPUTATIONS

The frequency mistuned pattern used for this study is shown in **Fig. 12**. The pattern has been obtained using a random number generator. The mode shape of blades is assumed to remain the same. In **Fig. 12** the y-axis is the amplitude of mistuning, which is defined as $(F_{max}-F_{min})/F_{ave}$, where F_{max}, F_{min} and F_{ave} are maximum, minimum and average frequencies respectively. For the case shown in **Fig. 12** the amplitude of mistuning is 6%.

Fig 12: Frequency mistuning pattern used in this study

Initially, the computations were performed for unstable mass flow of m=0.93. **Fig. 13** shows the time history of displacement for 4 blades around the assembly for the tuned and the mistuned fan assemblies. It is seen that the addition of mistuning pattern of **Fig. 12** has made the blade stable. On comparison with **Fig. 7**, it is seen that the time history of mistuned assembly at m=0.93 is very similar to tuned system at m=0.98. This suggests that the introduction of mistuning stops the initial disturbance from propagating round the circumference.

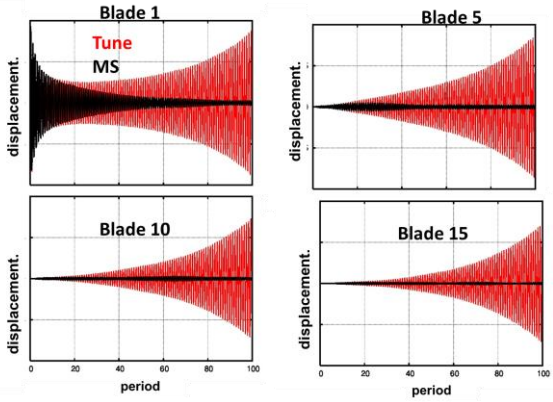

Fig 13: Time history of displacement for 4 blades around the annulus at m=0.93

This observation is further evident from the plots of **Fig 14** which shows the displacement plotted as a function of blade number for 5 instants of time during the motion for the tuned and the mistuned cases.

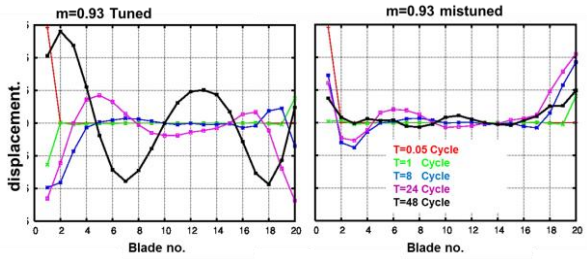

Fig 14: Time history of displacement as a function of blade number

The FFT of displacement around the circumference after 100 cycles for the tuned and mistuned systems is shown in **Fig. 15**. It is seen from this plot that for the tuned system the 2ND is the only mode present, whereas for the mistuned system there is response at in 1-4 NDs. It should be noted that the mistuned plot curve in **Fig. 15** has been multiplied by 5 so that it is visible in the plot.

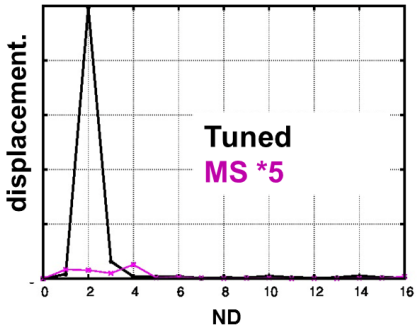

Fig 15: Fourier transform of displacement along the circumference

The time histories for mistuned system show a non-linear behaviour as can be seen from **Fig. 13** and **Fig. 16**. It can be seen from Fig. 16 that both blades respond in range of frequencies around the average frequency. Moreover, low frequency components are present in the response which is a due to interaction between blades.

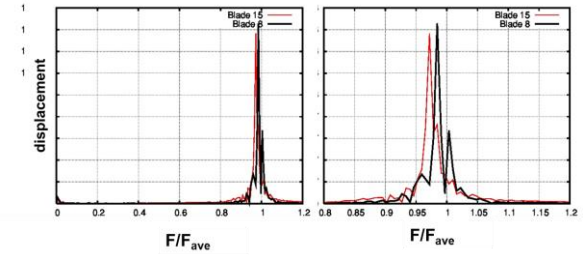

Fig 16: Fourier transform of time history displacement for two blade for mistuned case.

Fig. 17, shows the computed aero damping plotted against mass flow for a tuned system and the frequency mistuned assembly of **Fig 12**. In this plot a negative damping represents flutter. The results show that for the tuned system as the mass flow decreases, there is a sharp drop in aero damping and the blade flutters at mass flows below 0.95. However, for the level of mistuning used in these computations the blade remains stable at all the mass flows and the fan blade stalls before it flutters. As shown, above the time history for the mistuned cases is non-linear and hence obtaining a damping from a non-linear curve is quite approximate. The mistuned damping of **Fig. 17** has been obtained from time history of blade 1 between 90-100 cycles.

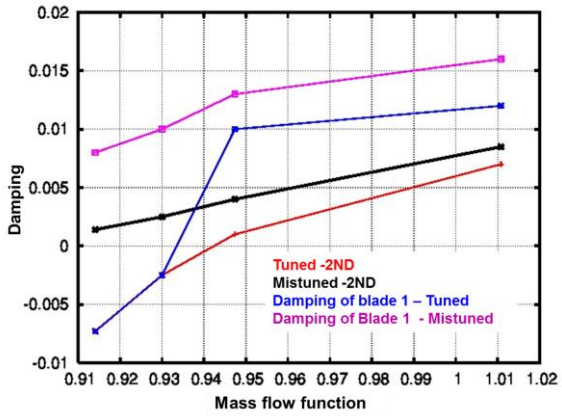

Fig 17: Comparison of aero damping for tuned and mistuned assembly

The effect of amplitude of mistuning on flutter at mass flows of m=0.91 and m=0.93 was considered next. **Fig 6** shows aero-damping plotted as a function of amplitude of mistuning. The amplitude of mistuning is defined as $(F_{max}-F_{min})/F_{ave}$, where F_{max}, F_{min} and F_{ave} are maximum, minimum and average frequencies respectively. For the pattern shown in **Fig. 12** the amplitude of mistuning is 6%. It should be noted that the same pattern of frequency mistuning is used in all the computations of this section and only the amplitude of mistuning (maximum frequency to minimum frequency) is changed. **Fig. 18** shows the aero damping of the fan assembly for m=0.91 and m=0.93 plotted against the amplitude of mistuning. The tuned system is shown as 0% mistuning level. It is seen from this plot that amplitude of mistuning has a significant effect on the aero damping of the assembly. For the pattern used, at m=0.91, a 3.2% amplitude is required for the blade to become stable, whereas for m=0.93 the amplitude is only 2%. Moreover, the aero damping of the blade asymptotes as the amount of mistuning is increased. Therefore, increasing mistuning will increase the flutter margin of a fan blade. A 2% mistuning level would bring the computed flutter boundary of **Fig. 1** much closer to the measured one.

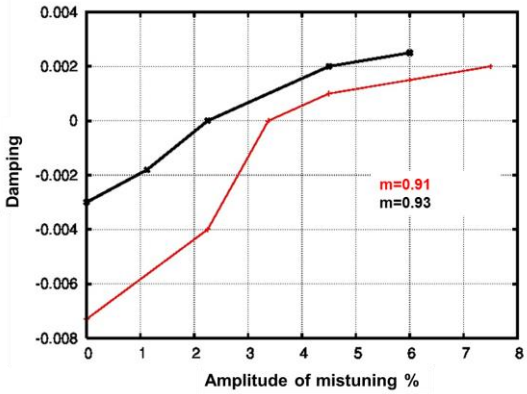

Fig 18: Aero damping as a function of amplitude of mistuning

Fig 19 which shows the displacement plotted as a function of blade number for 3 instants of time during the motion for an unstable mistuned case (m=0.91 and 1% amplitude of mistuning). It is seen from this figure that in the presence of mistuning instability will occur in more than one nodal diameter.

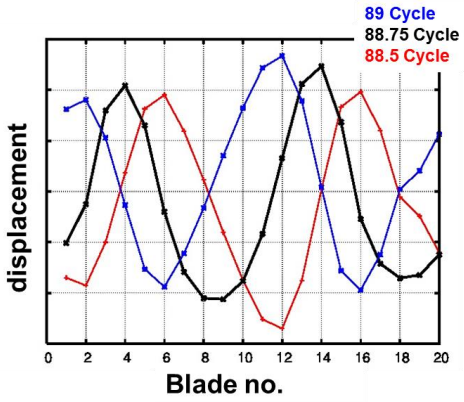

Fig 19: Time history of displacement as a function of blade number for an unstable mistuned case

Figure 20 shows the FFT of displacement around the circumference. It clearly shows the presence of 1, 2, 3 and 4 NDs is the response.

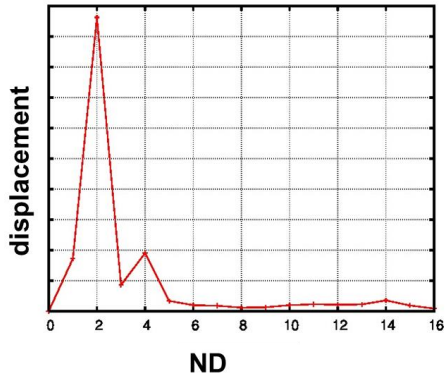

Fig 19: FFT of displacement around the circumference for an unstable mistuned case

CONCLUSIONS AND FUTURE WORK

The results clearly show that mistuning has a substantial effect on flutter stability of the fan blade and can increase the flutter margin of a fan blade significantly. Computed CFD results show that using a 2% random mistuning pattern will bring the computed and measured flutter boundary closer together. Initial results suggest that the amplitude of mistuning has much bigger influence on damping than the pattern of mistuning. Moreover, for points at lower flow, the amplitude of mistuning has to increase to guarantee blade stability. However, non-linear whole assembly, aeroelastic computations with mistuning require large amount of CPU time and faster models such as the one suggested in [1, 13] are required. In a future work, the results obtained in this work will be compared to those obtained from influence coefficient model of [1].

Acknowledgements

The authors thank Rolls-Royce plc for both sponsoring this work and allowing its publication. The first author also wishes to acknowledge support from UK TSB under the SILOET project. They gratefully acknowledge the contribution of their colleagues at Rolls-Royce plc: J. Green, R. Brooks, M. Wilson, and K. Johal.

REFERENCES

[1] Kielb, R. E., Feiner, D. M., Griffn, J. H., and Miyakozawa, T., 2004. , "Flutter of mistuned bladed disks and blisks with aerodynamic and FMM structural coupling". Proceedings of the ASME Turbo Expo 2004, Vienna, Austria, June 14–17, 2004, 6, pp. 573-579.

[2] Kielb, R. E., Feiner, D. M., Griffn, J. H., and Miyakozawa, T., March,2005. "Probabilistic analysis of mistuned bladed disks and blisks with aerodynamic and fmm structural coupling". 9th National Turbine Engine HCF Conference.

[3] Miyakozawa, T, 2008, "Flutter and forced response of turbomachinery with frequency mistuning and aerodynamic asymmetry", PhD thesis, Department of Mechanical Engineering and Materials Science Duke University

[4] Campobasso, M., and Giles, M., 2000. "Flutter and forced response of mistuned turbomachinery", Oxford University Computing Laboratory Report NA 00/20.

[5] Sladojevic, J., Petrov, E., Sayma, A., Imregun, M., and Green, J., 2005. "Investigation of the influence of aerodynamic coupling on response levels of mistuned bladed discs with weak structural coupling". Proceedings of the ASME Turbo Expo, 4, pp. 543 - 551.

[6] He, Z., Epureanu, B. I., and Pierre, C., 2007. "Fluid-structural coupling effects on the dynamics of mistuned bladed disks". AIAA Journal, 45(3), pp. 552 - 561

[7]Sayma, A. I., Vahdati, M., Sbardella, L., and Imregun, M., 2000, "Modeling of Three-Dimensional Viscous Compressible Turbomachinery Flows Using Unstructured Hybrid Grids," AIAA J., 38(6), pp. 945–954

[8] Spalart, P. R., and Allmaras, S. R., 1992, "A One-Equation Turbulence Model for Aerodynamic Flows," AIAA Paper No. 92-0439

[9] Vahdati, M., and Cumpsty, N. A., 2012, "Mechanisms for Wide-Chord Fan Blade Flutter," 13th International Symposium on Unsteady Aerodynamics, Aeroacoustics and Aeroelasticity of Turbomachines, University of Tokyo, Japan, Sept. 11–14, Paper No. ISUAAAT 13-I-5.

[10] Choi, M., Smith, N.H.S and Vahdati. M, 2013, "Validation of numerical simulation for rotating stall in a transonic fan", Journal of turbomachinery 135 (2), 021004

[11] J Dodds, J., Vahdati, M., 2015, "Rotating Stall Observations in a High Speed Compressor—Part II: Numerical Study" , Journal of Turbomachinery 137 (5), 051003

[12]Vahdati, M, Smith, N.H.S, Zhao, F.,2015, "Influence of Intake on Fan Blade Flutter", Journal of Turbomachinery 137 (8), 081002

[13] Kielb, R. E., Hall, K. C., Hong, E., and Pai, S. S., 2006, "Probabilistic Flutter Analysis of a Mistuned Bladed Disks," ASME Paper No. GT2006-90847, Barcelona, Spain, May 8-11, 2006